analytical chemistry

Article

Cite This: *Anal. Chem.* 2019, 91, 15846−15852

pubs.acs.org/ac

# Dual-Mode Electrochemical Assay of Prostate-Specific Antigen Based on Antifouling Peptides Functionalized with Electrochemical Probes and Internal References

Caifeng Ding, Xinyan Wang, and Xiliang Luo*

Key Laboratory of Optic-electric Sensing and Analytical Chemistry for Life Science, Ministry of Education; Shandong Key Laboratory of Biochemical Analysis; Key Laboratory of Analytical Chemistry for Life Science in Universities of Shandong; and College of Chemistry and Molecular Engineering, Qingdao University of Science and Technology, Qingdao 266042, P.R. China

Supporting Information

**ABSTRACT:** Sensitive and selective detection of target analytes in complex biological samples is currently a major challenge. Herein we constructed a dual-mode antifouling electrochemical sensing platform for the detection of prostate-specific antigen (PSA) based on two kinds of antifouling peptides functionalized with a graphene oxide−$Fe_3O_4$−thionine (GO-$Fe_3O_4$-Thi) probe and internal reference ferrocene (Fc), respectively. The longer peptide (Pep1) modified with the GO-$Fe_3O_4$-Thi probe was designed to contain a peptide sequence (HSSKLQK) capable of being recognized and cut by PSA. The GO-$Fe_3O_4$-Thi probe functions not only as a peroxidase mimick (GO-$Fe_3O_4$) but also works as an electrochemical probe due to the presence of thionine (Thi). The concentration of PSA can be measured through both the increase of differential pulse voltammetry (DPV) signal change of Thi and the decrease of chronoamperometry (CA) signal of the reduction of $H_2O_2$ electrocatalyzed by GO-$Fe_3O_4$. The shorter peptide (Pep2) was tagged with Fc, whose DPV signal remained constant and was independent of the presence of PSA, and it was used as an internal reference to ensure the reliability and accuracy of the measurement. The dual-mode PSA sensor exhibits a wide linear range from 5 pg/mL to 10 ng/mL, with low detection limits of 0.76 and 0.42 pg/mL through DPV and CA modes, respectively. More importantly, owing to the antifouling capability of the designed peptides, the biosensor performances remained operable even in human serum, indicating feasibility of the electrochemical biosensor for practical PSA quantification in complex samples.

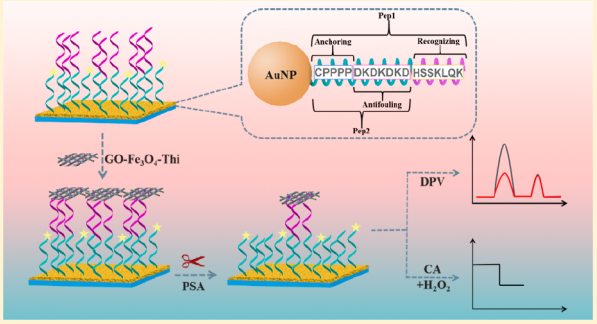




Prostate-specific antigen (PSA) is an androgen-regulated serine protease, and it is the most important serum biomarker for preoperative diagnosis and screening of prostate cancer.[1−4] When the concentration of PSA reaches 2 ng/mL, it is generally considered to indicate the risk of prostate cancer, and 4 ng/mL is the critical value in serum.[5,6] PSA detection below 0.1 ng/mL is necessary to monitor response and recurrence of anti-CaP drugs in patients undergoing radical prostatectomy.[7,8] In addition, PSA is found in the serum of breast cancer patients and is being explored as a target for breast cancer screening.[9] Because PSA concentrations in women's serum are much lower than in men's, it is important to develop an ultrasensitive method for determining PSA in serum for the early diagnosis of breast cancer.[10] Alot of methods for the determination of PSA have been developed such as colorimetric,[11,12] fluorescence,[13] surface-enhanced Raman scattering,[14] electrochemistry,[15] chemiluminescence,[16] and electrogenerated chemluminescence (ECL),[17,18] which are mainly based on specific antibody−antigen recognition. Denmeade et al.[19] identified a specific peptide with the amino acid sequence HSSKLQ, which could be used as a substrate to measure PSA enzymatic activity in extracellular fluid with high specificity and good stability. Zhao et al.[20] developed an electrochemical biosensor based on ferrocene-functionalized helical peptide (CHSSKLQK) that directly emitted an electrochemical signal using a peptide cleavage event to detect PSA in a simple and sensitive manner.

In recent years, electrochemical biosensors have been widely used to detect tumor markers due to the high sensitivity and low cost. However, these biosensors face challenges of unspecific adsorption of biomolecules in the complex environment, especially in the detection of actual samples, and the general approach to alleviating this challenge is to integrate target recognition into another antifouling surface. In recent years, many antifouling materials, such as polyethylene glycol (PEG),[21,22] zwitterionic polymers,[23,24] and antifouling peptides,[25−29] have been widely used in electrochemical biosensors and have shown good selectivity in complex environments. Among them, zwitterionic peptides have outstanding biocompatibility and can be synthesized as

**Received:** September 16, 2019
**Accepted:** November 18, 2019
**Published:** November 18, 2019




DOI: 10.1021/acs.analchem.9b04206
*Anal. Chem.* 2019, 91, 15846−15852

desired. Nowinski et al.[30] designed an antifouling zwitterionic peptide (EKEKEKE-PPPPC) and demonstrated that its well-defined secondary structure could form a denser single layer with modified antifouling properties.

Graphene oxide (GO), a two-dimensional structure material, has attracted much attention in materials science and biotechnology due to its large surface area as well as remarkabe mechanical, electrical, and thermal properties.[31,32] Song et al.[33] reported that GO has peroxidase-like activity, and Wei et al.[34] reported that $Fe_3O_4$ as a peroxidase mimetic can be used to detect $H_2O_2$ and glucose. Based on the excellent properties of GO and magnetic nanoparticles, the composite materials formed by them can greatly improve their peroxidase-like activity, so it can generate strong electrochemical (EC) signals via chronoamperometry (CA) detection.[35,36] The electrochemical probe thionine (Thi) can be conjugated to the surface of GO by $\pi-\pi$ interaction to obtain GO-$Fe_3O_4$-Thi nanocomposites,[37,38] and the electrochemical response can be measured by differential pulse voltammetry (DPV).

To eliminate the interference from external factors, internal standard molecules were used to construct biosensors to ensure the reliability and accuracy of the measurement.[39−41] Herein we constructed an electrochemical biosensor based on two kinds of functional peptides and internal standard molecules for the detection of PSA. GO-$Fe_3O_4$-Thi nanocomposites are modified to the longer peptide as DPV and CA probes. Fc, which is used as the internal standard molecule, is tagged to the terminus of the shorter peptide. The concentration of PSA could be measured through both the ratio of DPV change between Thi and Fc, and the CA signal of the reduction of $H_2O_2$ electrocatalyzed by GO-$Fe_3O_4$. Except as the carriers of the electrochemical probes, the same parts of the two kinds of peptides are designed to have the antifouling property, so nonspecific adsorption can be avoided and the fabricated biosensor shows high selectivity and sensitivity.

## EXPERIMENTAL SECTION

**Materials and Reagents.** Chloroauric acid ($HAuCl_4$), hydrogen peroxide ($H_2O_2$), thionine (Thi), ferric chloride hexahydrate ($FeCl_3·6H_2O$), ferrous sulfate heptahydrate ($FeSO_4·7H_2O$), ammonia ($NH_3·H_2O$), 1-ethyl-3-(3-(dimethylamino)propyl)carbodiimide hydrochloride (EDC), *N*-hydroxysulfosuccinimide sodium salt (NHS), and thrombin (TB) were purchased from Sigma-Aldrich Chemical Co. (St. Louis, MO). Graphene oxide (GO) was purchased from Nanjing XFNANO Co., Ltd. (Nanjing, China). The peptides ($NH_2$-KQLKSSHDKKDKDPPPPC, Pep1; Fc-DKDKDKDPPPPC, Pep2-Fc) and tris(2-carboxyethyl)-phosphine hydrochloride (TCEP) were obtained from Sangon Biotech Co., Ltd. (Shanghai, China). Indium tin oxide (ITO)-coated glass slides were purchased from NanoSci Inc. (China). Prostate specific antigen (PSA) was purchased from Shanghai Linc-Bio Science Co., Ltd. (Shanghai, China). Fetal bovine serum (FBS), bovine serum albumin (BSA), carcinoembryonic antigen (CEA), and human alpha fetoprotein (AFP) were purchased from Beijing Bo Yang Hongda Technology Co. Ltd. (Beijing, China). HeLa cells and HUVEC cells were purchased from KeyGEN BioTECH Co. (China). Clinical human serum samples were supplied by the Eighth People's Hospital of Qingdao. Other chemicals were of analytical grade and ordered from Aladdin Reagent Co. Ltd. A 10 mM phosphate buffer solution (PBS) (pH = 7.4) and a 0.1 M phosphate buffer solution (PBS) (pH = 7.4) were used as the buffer solutions.

**Apparatus.** Chronopotentiometry (CA), cyclic voltammetric (CV), and differential pulse voltammetry (DPV) measurements were conducted with a CHI 660E electrochemistry workstation (Shanghai CH Instruments, China). All experiments were performed with a modified glassy carbon electrode as the working electrode, a Ag/AgCl (saturated KCl) as reference electrode, and a platinum wire as counter electrode. The scanning electron micrographs (SEM) were taken with a JEOL JSM-7500F (Hitachi High-Technology Co., Ltd., Japan). The morphology and structure were characterized by a transmission electron microscope (TEM) (USA). The Fourier transform infrared spectra were obtained with a Nicolet 510P FTIR spectrophotometer (Thermo Nicolet, USA). Fluorescence spectroscopy was measured on a F-2700 spectrometer (Hitachi, Japan). The fluorescence confocal imaging was monitored using a TCS SP5 confocal laser microscope (Leica, Germany). Hydrophilicity characterizations of different modified surfaces were performed on a static water contact angle (WCA) measurement (Shanghai Zhongchen Instrument Co., China). Zeta potential measurement of the peptides was performed with a Zetasizer Nano-ZS (Malvern Instruments, Malvern, UK).

**Fabrication of the AuNP-Based Sensing Interface.** After the ITO electrode (0.5 cm × 3.0 cm) was ultrasonically washed in absolute acetone, ethanol, and water sequentially for 20 min, a typical electrochemical polymerization was conducted by scanning five cycles from −0.9 V to +0.5 V at a scan rate of 50 mV/s in a mixed aqueous solution containing 1 mM $HAuCl_4$ and 0.5 M NaCl. The AuNP-modified electrode was obtained after drying at room temperature.

**Preparation of the GO-$Fe_3O_4$-Thi Nanocomposites.** The amount was optimized with reference to the previous synthesis method.[42] GO-$Fe_3O_4$ was synthesized from GO suspension (40 mg) in 10 mL solution of 37.2 mg of $FeCl_3·6H_2O$ and 19.2 mg of $FeSO_4·7H_2O$ at 80 °C under $N_2$. A mixed water solution of $FeCl_3$ and $FeSO_4$ was added slowly to the GO suspension, and the ammonia solution was added quickly to precipitate $Fe^{2+}/Fe^{3+}$ ions for the synthesis of magnetite ($Fe_3O_4$) particles. The temperature was raised to 85 °C, and a 30% ammonia solution was added to adjust the pH to 10. After being rapidly stirred for 45 min, the solution was cooled to room temperature. The product was magnetically washed with Milli-Q water twice and dried in a vacuum. Then the GO-$Fe_3O_4$ composites were prepared. A total of 2 mg of GO-$Fe_3O_4$ was added into 1 mL of Thi solution (1 mM), and the mixture was agitated ultrasonically for 2 h. After being washed by magnetic separation and dried in a vacuum, the GO-$Fe_3O_4$-Thi nanocomposites were obtained.

**Construction of the Electrochemical Sensing Surface.** The modified electrode was incubated 12 h in phosphate-buffered saline (PBS, 0.1 M, pH 7.4) containing 0.2 mg/mL multifunctional peptides and 10 mM TCEP at 4 °C, and the volume ratio of the two peptides was 4:1 after optimization. EDC (0.1 M) and NHS (0.01 M) were dissolved in GO-$Fe_3O_4$-Thi nanocomposites and incubated at room temperature to activate the carboxyl groups of GO-$Fe_3O_4$-Thi for 1 h. Subsequently, the peptides/AuNPs/ITO electrode was inserted into the activated GO-$Fe_3O_4$-Thi solution for 2 h to construct the sensing surface of GO-$Fe_3O_4$-Thi/Peptides/AuNPs/ITO, and then the sensing surface was washed three times with 10 mM PBS buffer.

**Electrochemical Measurements.** The PSA standard solutions at different concentrations were transferred to the



DOI: 10.1021/acs.analchem.9b04206
*Anal. Chem.* 2019, 91, 15846−15852

**Scheme 1. Antifouling Electrochemical Biosensor Working Principle**

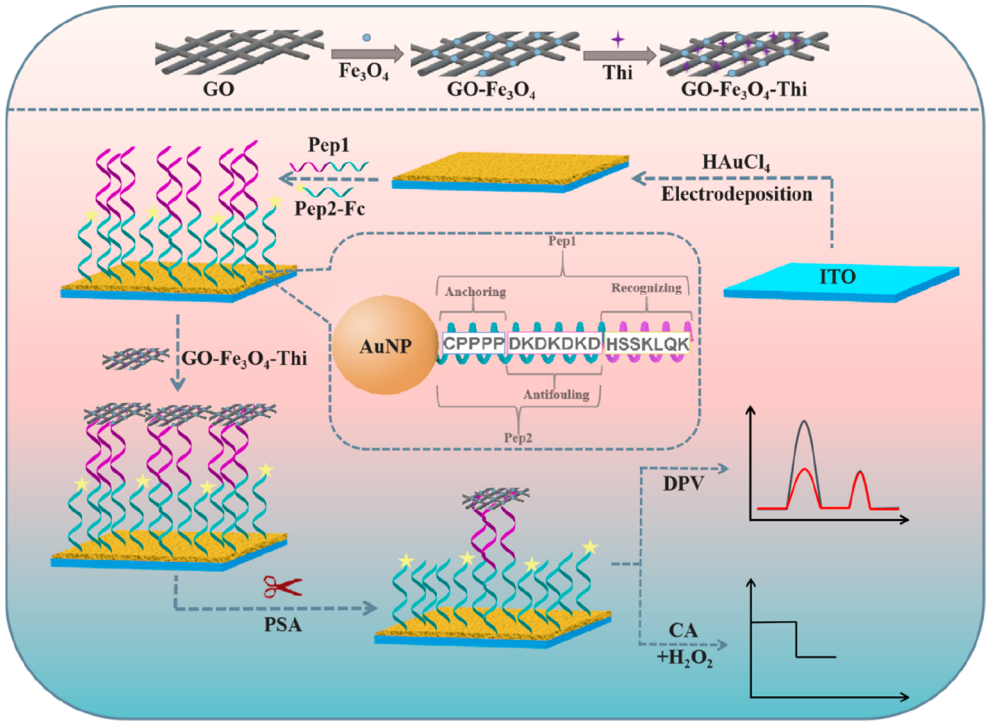


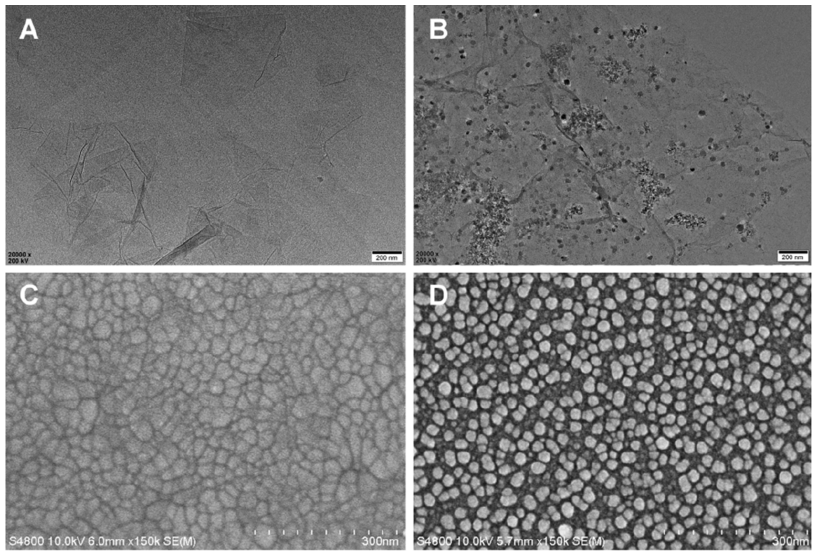


**Figure 1.** TEM images of GO (A) and GO-$Fe_3O_4$ nanocomposites (B), and SEM images of bare ITO (C) and AuNPs/ITO (D).

sensing surface of GO-$Fe_3O_4$-Thi/peptides/AuNPs/ITO to incubate for 40 min (Figure S1B). After washing with PBS buffer three times, the biosensor tested through DPV was scanned from −0.5 to 0.5 V directly in 0.1 M PBS solution, and the peak currents were first recorded. Subsequently, the CA method was scanned at a potential of −0.4 V. After the background signal remained stable, 100 $\mu$L of 5 M $H_2O_2$ was injected into the PBS solution under mild stirring.

## RESULTS AND DISCUSSION

**Response Mechanism of the Antifouling Electrochemical Biosensor.** Scheme 1 shows the dual-mode electrochemical biosensor for the detection of PSA based on the two kinds of antifouling peptides and internal standard method. First, Thi could be attached onto the GO-$Fe_3O_4$ surface via $\pi-\pi$ stacking to obtain the GO-$Fe_3O_4$-Thi nanocomposites, which serve as an excellent electrochemical probe because of high specific surface characteristics and unique electronic properties. Then the electrode is modified with AuNPs by electropolymerization to improve the conductivity and provide binding sites for the peptides. Pep1 and Pep2-Fc are immobilized onto the AuNPs through Au−S bonds. The GO-$Fe_3O_4$-Thi nanocomposites are immobilized at the other end of Pep1 through amide bonds. In the presence of PSA, one part of Pep1 can be recognized and cut off. Then the GO-$Fe_3O_4$-Thi nanocomposites leave the surface of the electrode and the DPV signal of Thi decreases. Fc, tagged on Pep2, which is used as an internal standard signal molecule,



DOI: 10.1021/acs.analchem.9b04206
*Anal. Chem.* 2019, 91, 15846−15852

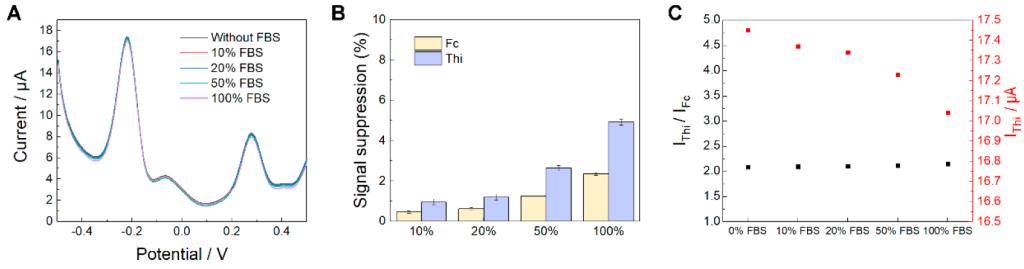


**Figure 2.** (A) DPV responses of the constructed sensing surfaces before and after incubation in different concentrations of FBS samples. (B) Antifouling property of the ferrocene (yellow) and Thi (purple) for FBS samples of different concentrations (V/V). (C) Plots of electrochemical response versus antifouling characteristics from Thi and Fc.

can eliminate the interference from the external environment and enhance the accuracy of the sensing platform. The ratio changes of the DPV signal of Thi and Fc can determine the concentration of PSA. Simultaneously, GO-$Fe_3O_4$ nanocomposites are demonstrated to possess intrinsic peroxidase-like activity and enhanced affinity toward $H_2O_2$, and the CA signal upon reduction of $H_2O_2$ electrocatalyzed by GO-$Fe_3O_4$ in the solution increases with the increase in PSA concentration. Dual-mode detection can then be realized. More importantly, the same parts of Pep1 and Pep2-Fc have the antifouling sequence, so the prepared biosensor is capable of detecting PSA in complex media, such as human serum, with significant selectivity.

**Characterization of GO-$Fe_3O_4$-Thi Nanocomposites.** Figure 1 shows the TEM images of GO and GO-$Fe_3O_4$ nanocomposites. The TEM image shows that the GO film is transparent and thin (Figure 1A), and the $Fe_3O_4$ nanoparticles are well dispersed on the surface (Figure 1B). The average size of the $Fe_3O_4$ nanoparticles is about 10−20 nm. The energy-dispersive spectrum of GO-$Fe_3O_4$ nanocomposites (Figure S1A) shows the successful synthesis of materials. The FTIR spectrum of GO-$Fe_3O_4$ nanocomposites (Figure S1B) differs from that of GO as evidenced by the more obvious band at 568 $cm^{-1}$. The new bands at 1459 and 1397 $cm^{-1}$ are assigned to the formation of either a monodentate complex or a bidentate complex between the carboxyl group and iron atoms on the surface of the magnetic nanoparticles, indicating that the $Fe_3O_4$ NPs are covalently bonded to GO. The fluorescence experiment gives further evidence of the assembly of Thi onto the GO-$Fe_3O_4$ surface (Figure S1C). Fluorescence emission at 617 nm of GO-$Fe_3O_4$-Thi (green line) is affirmed to arise from Thi, according to the individual Thi emission (blue line), suggesting that Thi is successfully attached to the GO-$Fe_3O_4$ surface.

**Characterization of the Developed Biosensing Interfaces.** The morphologies of AuNPs were characterized by SEM as shown in Figure 1. Compared with the bare ITO electrode (Figure 1C), the AuNPs are found on the ITO surface (Figure 1D), and the size of AuNPs is about 15−20 nm. DPV was used to ensure the assembly process in the presence of a solution-phase redox probe response (Figure S2A), and the signal characteristic peak of Fc appeared when the peptides were immobilized onto the AuNPs (blue line). After the GO-$Fe_3O_4$-Thi attachment to Pep1, the characteristic signal peak of Thi also appeared (green line). As shown in Figure S2B, after incubation in PSA solution for 40 min, the fluorescence of Thi can be detected in the solution, further proving the feasibility of the experiment.

Hydrophilicity and wetting characteristics were mapped through static water contact angle assessment. As shown in Figure S3 and Table S1, due to the hydrophilicity of the peptides, the water contact angle of peptides/Au/ITO decreases from 75.16° to 39.38°. Subsequent GO-$Fe_3O_4$-Thi coupling (GO-$Fe_3O_4$-Thi/peptides/Au/ITO) is associated with a further significant increase in wetting (WCA 25.74°).

**Generic Antifouling Characteristics.** To enable effective antifouling character, it has been established that molecular films should be highly hydrophilic and of low net charge. The isoelectric point (pI) of Pep2 is 6.4. As shown in Figure S4A, the resolved zeta potential of Pep2 solution was pleasingly close to 0.0 mV. Pep1 and Pep2-Fc carry a small amount of negative or positive charges, and their zeta potential are −0.84 mV and 4.54 mV (Figure S4B and Figure S4C), slightly deviated from electrical neutral, which would not impact the biosensor's antifouling performance.

To evaluate the antifouling ability of the constructed sensing surfaces, the DPV responses of the interfaces were compared before and after incubation in FBS for 30 min, and the DPV resolved signal decrease directly indicates nonspecific association. As shown in Figure 2A and Figure 2B, after incubation in 100% FBS, the DPV signal reduction of Fc and Thi is about 2.35% and 4.92%, respectively. This result demonstrates the good antifouling ability of the peptide-based biosensor interface, which is further verified by fluorescein diacetate (FDA) labeled cells (Figure S5). As shown in Figure 2C, the signal of Thi decreased gradually, but the ratio of $I_{Thi}/I_{Fc}$ remained almost constant, which indicated the importance of internal standard method. Due to the better biocompatibility of AuNPs, there are more cells that can be seen on the Au/ITO surface than on the bare ITO electrode. After modification of the electrode with peptides, only a few cells are observed at the surface.

**Optimization of the Proposed Biosensor.** The DPV and CA signal of the proposed biosensor is influenced by many factors. To obtain high sensitivity and good antifouling performance, experiments are performed to optimize the dosage of the two peptides (Figure S6A), and the best volume ratio of the two peptides is 4:1. As shown in Figure S6B, the change of the DPV signal increases with the increase of the PSA incubation time from 10 to 40 min. When the incubation time is prolonged from 40 to 60 min, the change of the DPV signal keeps nearly stable, due to the saturated binding between the peptide and PSA. Therefore, 40 min of incubation time is used for the detection of PSA.

**Electrochemical Detection of PSA.** The prepared antifouling electrochemical biosensor was used for the quantitative detection of PSA under the optimal conditions.



DOI: 10.1021/acs.analchem.9b04206
Anal. Chem. 2019, 91, 15846−15852

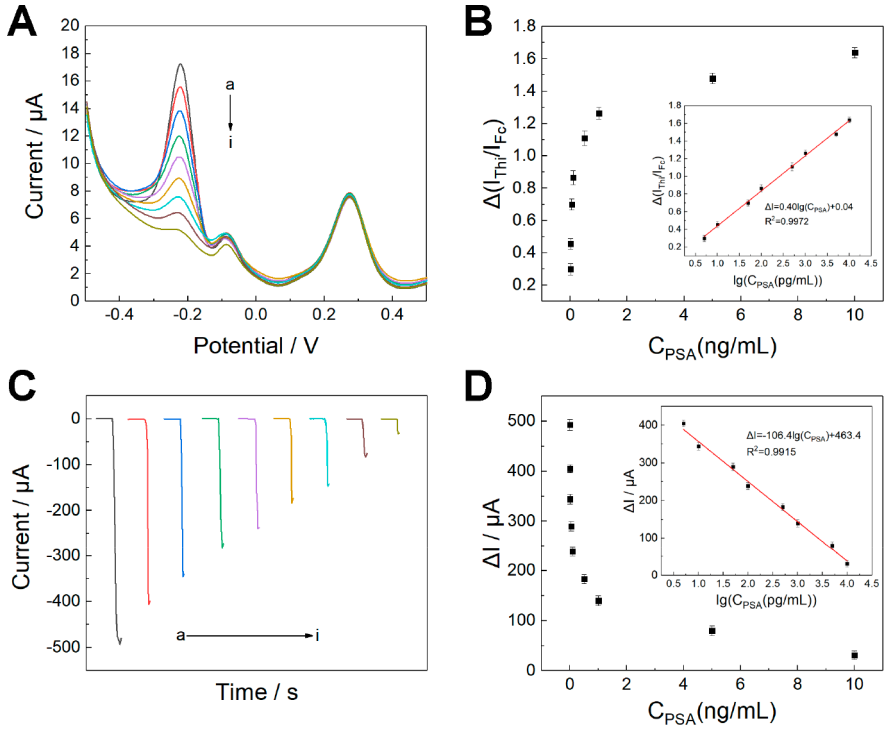


**Figure 3.** (A) DPV resolved responses of the sensor interfaces to PSA at concentrations from 5 pg/mL to 10 ng/mL. (B) Calibration curve of the PSA and the signal suppression ($R^2$ = 0.997). (C) CA resolved responses of the sensor interfaces to PSA at concentrations from 5 pg/mL to 10 ng/mL. (D) Calibration curve of the PSA and the signal suppression ($R^2$ = 0.991).

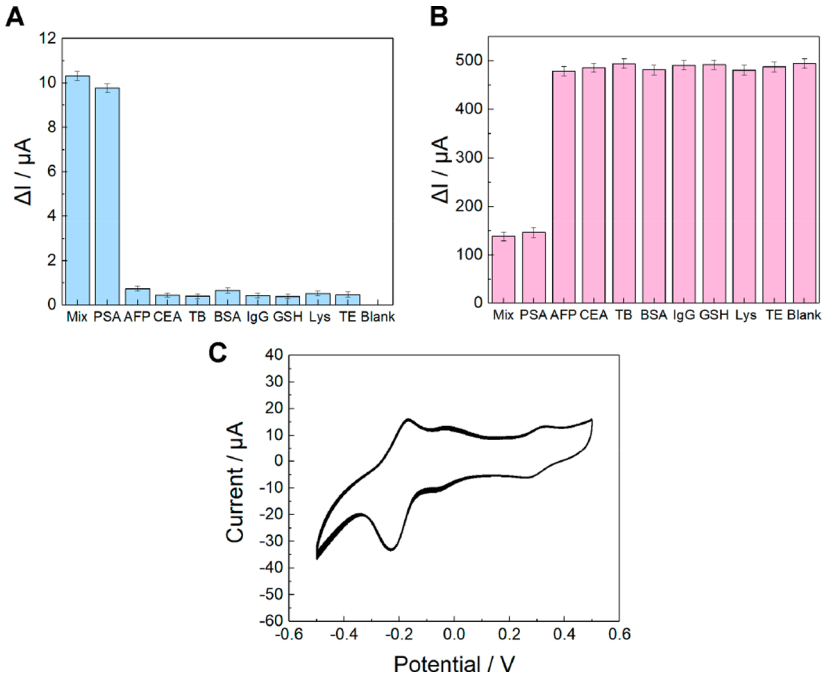


**Figure 4.** DPV (A) and CA (B) methods: selectivity of the biosensor after incubation with different kinds of proteins: PSA (1.0 ng/mL), AFP (10.0 ng/mL), CEA (10.0 ng/mL), TB (10.0 ng/mL), BSA (10.0 ng/mL), IgG (10.0 ng/mL), GSH (10.0 ng/mL), Lys (10.0 ng/mL), TE (10.0 ng/mL), and blank. (C) Stability of the prepared biosensor.

From Figure 3A we can see that the DPV signal of Thi decreases with the increase in PSA concentration while the signal of Fc keeps almost constant, which is the same as for the internal standard method. As shown in Figure 3B, $\Delta(I_{Thi}/I_{Fc})$ is in a linear relationship with the PSA concentration within the range from 5 pg/mL to 10 ng/mL with a correlation coefficient of 0.997. The regression equation is $\Delta I$ = 0.40 lg($C_{PSA}$) + 0.04 (pg/mL), where $\Delta I$ is the current change, and $C$ is the PSA concentration. The correlation coefficient becomes 0.991 without the internal standard signal molecule (Fc) as shown in Figure S7. The correlation coefficient of the biosensor without the internal standard signal molecule is



DOI: 10.1021/acs.analchem.9b04206
*Anal. Chem.* 2019, 91, 15846−15852

lower than the one with the internal standard signal molecule, showing that using the internal standard method can make the measurement accuracy higher.

The concentration of PSA can also be detected through the increase of the CA of $H_2O_2$ reduction catalyzed by GO-$Fe_3O_4$ as shown in Figure 3C. Figure 3D shows that the CA signal is in a linear relationship with the PSA concentration within the range from 5 pg/mL to 10 ng/mL with a correlation coefficient of 0.991. The regression equation is $\Delta I = -106.4 \lg(C_{PSA}) + 463.4$ (pg/mL), where $\Delta I$ is the current change, and $C$ is the PSA concentration. The detection limits of the two modes are 0.76 pg/mL and 0.42 pg/mL (where S/N = 3), respectively, and both are lower than many previous reports (Table S2). The detection limit of the method without internal standard is about 1.34 pg/mL (where S/N = 3), which is a little higher than the method with internal standard. The DPV signal is generated by Thi itself, without the addition of other electron transfer mediators. At the same time, the GO-$Fe_3O_4$ displays high electrocatalytic activity toward the reduction of $H_2O_2$ without peroxidase to improve the sensitivity of the biosensor. Lastly, the double signal can mutually authenticate to get accurate detection results. But the measurement accuracy of the CA method is a little lower than that of the DPV method because of the absence of the internal standard signal molecule. The fluorescence intensity of the Thi departing from the surface of the electrode to the solution also shows the relationship to the concentration of PSA (Figure S8).

**Specificity and Stability of the Biosensor.** To evaluate the specificity of the electrochemical biosensor, we challenged the biosensor with other possible interferences such as alpha fetoprotein (AFP), carcinoembryonic antigen (CEA), thrombin (TB), bovine serum albumin (BSA), immunoglobulin G (IgG), glutathione (GSH), lysozyme (Lys), and telomerase (TE) under the same conditions. The biosensor was incubated with 10.0 ng/mL AFP, CEA, TB, BSA, IgG, GSH, Lys, and TE, 1.0 ng/mL PSA, and the mixture of all. Compared with other proteins, a large increase in the change of the DPV signal is observed for 1.0 ng/mL PSA while very slight changes are found for the other tested proteins (Figure 4A, $\Delta I = I_0 - I_1$, $I_0$ is the current value of Thi before reaction and $I_1$ is the current value of Thi after reaction). As shown in Figure 4B, the CA intensity after incubation with PSA becomes low while that with other proteins is still high. The results indicate that the biosensor has excellent selectivity for the detection of PSA ($\Delta I = 0 - I_a$, $I_a$ is the current value after added $H_2O_2$). Stability analysis of the biosensor was performed by continuous CV measurement in PBS (0.1 M, pH 7.4). As shown in Figure 4C, the redox peaks of Fc and Thi are at about +0.3 V and −0.2 V, respectively, and the converted signal of CV is substantially unchanged after 50 cycles. This proves that stability and intrareproducibility of the biosensor are excellent. We used five different electrodes to prove the inter-reproducibility of the biosensor, and the relative standard deviation was about 3.1%.

**Clinical Serum Sample Analysis.** The proposed method was also implemented in the analysis of clinical serum samples, which were provided by Affiliated Hospital of Heze Medical College. The assay results are listed in Table 1. From the results in the table we can see that the relative error (<11.5%) for this method without internal standard is much higher than this method with internal standard (<5.1%), showing the better measurement accuracy due to the usage of the internal standard. The obtained results showed an acceptable agreement with the data provided by Affiliated Hospital of Heze Medical College using the ECL method, indicating a possibility for clinical application.

**Table 1. Analytical Results of PSA in Clinical Serum Samples**

| | ECL method (ng/mL) | this method (ng/mL)[a] | relative error (%) | the method without internal standard (ng/mL)[a] | relative error (%) |
|---|---|---|---|---|---|
| DPV | 1.57 | 1.53 | −2.5 | 1.39 | −11.5 |
| | 5.31 | 5.37 | 1.1 | 4.93 | −7.2 |
| | 8.23 | 7.81 | −5.1 | 7.48 | −9.1 |
| CA | 1.57 | 1.66 | 5.7 | | |
| | 5.31 | 5.48 | 3.2 | | |
| | 8.23 | 8.63 | 4.9 | | |

[a]Average value of five measurements.

## CONCLUSIONS

In summary, a dual-mode and low fouling electrochemical PSA biosensor was constructed based on antifouling peptides loaded with internal references and electrochemical probes. Within the designed assaying system, Thi provided a sensitive DPV current response originating from its redox reaction, and GO-$Fe_3O_4$ with good catalytic ability for $H_2O_2$ reduction produced a significantly enhanced CA signal, while the Fc as internal reference ensured the reliability and accuracy of the assay. These unique biosensing performances, in addition to the excellent antifouling ability due to the presence of antifouling zwitterionic peptides on the sensing interface, make this assay a highly attractive method for the detection of PSA in human serum samples. It is also expected that the strategy for the construction of this biosensor may be extended to the development of other sensitive, accurate, and antifouling electrochemical biosensors.

## ASSOCIATED CONTENT

### Supporting Information

The Supporting Information is available free of charge at https://pubs.acs.org/doi/10.1021/acs.analchem.9b04206.

Characterization of GO-$Fe_3O_4$-Thi nanocomposites (Figure S1), construction process and the feasibility of the biosensor (Figure S2), static water contact angles of the developed biosensing interfaces (Figure S3 and Table S1), optimization of the experimental conditions (Figure S4), zeta potentials (Figure S5), generic antifouling characteristics of the developed biosensing interfaces (Figure S6), electrochemical detection of PSA without internal standard and fluorescence detection of PSA (Figure S7), and comparison with other reports (Table S2) (PDF)

## AUTHOR INFORMATION


### Corresponding Author

*E-mail: xiliangluo@qust.edu.cn. Fax: +86 532 8402 2860.

### ORCID

Caifeng Ding: 0000-0002-5281-0158

Xiliang Luo: 0000-0001-6075-7089


### Notes

The authors declare no competing financial interest.



DOI: 10.1021/acs.analchem.9b04206
Anal. Chem. 2019, 91, 15846−15852

## ■ ACKNOWLEDGMENTS

The authors greatly acknowledge support from the Project Fund for Shangdong Key R&D Program (2017GGX20121), the National Natural Science Foundation of China (grant 21675093), and the Taishan Scholar Program of Shandong Province of China (grant ts20110829). The authors thank Dr. Mingjing Zou (The Affiliated Hospital of Heze Medical College) for assistance with real sample assay in the hospital.

## ■ REFERENCES

(1) Nam, J. M.; Thaxton, C. S.; Mirkin, C. A. *Science* **2003**, *301*, 1884−1886.
(2) Thaxton, C. S.; Elghanian, R.; Thomas, A. D.; Stoeva, S. I.; Lee, J. S.; Smith, N. D.; Schaeffer, A. J.; Klocker, H.; Horninger, W.; Bartsch, G.; Mirkin, C. A. *Proc. Natl. Acad. Sci. U. S. A.* **2009**, *106*, 18437−18442.
(3) Hearty, S.; Leonard, P.; O'Kennedy, R. *Nat. Nanotechnol.* **2010**, *5*, 9−10.
(4) Zhang, H.; Zhao, Q.; Li, X. F.; Le, X. C. *Analyst* **2007**, *132*, 724−737.
(5) He, Y.; Xie, S.; Yang, X.; Yuan, R.; Chai, Y. *ACS Appl. Mater. Interfaces* **2015**, *7*, 13360−13366.
(6) Chikkaveeraiah, B. V.; Bhirde, A. A.; Morgan, N. Y.; Eden, H. S.; Chen, X. *ACS Nano* **2012**, *6*, 6546−6561.
(7) Chang, H.; Kang, H.; Ko, E.; Jun, B.; Lee, H.; Lee, Y.; Jeong, D. *ACS Sens.* **2016**, *1*, 645−649.
(8) De Angelis, G.; Rittenhouse, H. G.; Mikolajczyk, S. D.; Blair Shamel, L.; Semjonow, A. *Rev. Urol.* **2007**, *9*, 113−123.
(9) Yu, H.; Giai, M.; Diamandis, E. P.; Katsaros, D.; Sutherland, D. J. A.; Levesque, M. A.; Roagna, R.; Ponzone, R.; Sismondi, P. *Cancer Res.* **1995**, *55*, 2104−2110.
(10) Qi, H.; Li, M.; Dong, M.; Ruan, S.; Gao, Q.; Zhang, C. *Anal. Chem.* **2014**, *86*, 1372−1379.
(11) Cao, C.; Li, X.; Lee, J.; Sim, S. J. *Biosens. Bioelectron.* **2009**, *24*, 1292−1297.
(12) Qu, F.l.; Li, T.; Yang, M. H. *Biosens. Bioelectron.* **2011**, *26*, 3927−3931.
(13) Liu, D. D.; Huang, X. L.; Wang, Z. T.; Jin, A.; Sun, X. L.; Zhu, L.; Wang, F.; Ma, Y.; Niu, G.; Hight Walker, A. R.; Chen, X. Y. *ACS Nano* **2013**, *7*, 5568−5576.
(14) Grubisha, D. S.; Lipert, R. J.; Park, H. Y.; Driskell, J.; Porter, M. D. *Anal. Chem.* **2003**, *75*, 5936−5943.
(15) Zhang, S. S.; Du, P.; Li, F. *Talanta* **2007**, *72*, 1487−1493.
(16) Zheng, Y.; Chen, H.; Liu, X. P.; Jiang, J. H.; Luo, Y.; Shen, G. L.; Yu, R. Q. *Talanta* **2008**, *77*, 809−814.
(17) Sardesai, N.; Pan, S. M.; Rusling, J. *Chem. Commun.* **2009**, *33*, 4968−4970.
(18) Sardesai, N. P.; Barron, J. C.; Rusling, J. F. *Anal. Chem.* **2011**, *83*, 6698−6703.
(19) Denmeade, S. R.; Lou, W.; Lovgren, J. *Cancer Res.* **1997**, *57*, 4924−4930.
(20) Zhao, N.; He, Y. Q.; Mao, X.; Sun, Y. H.; Zhang, X. B.; Li, C. Z.; Lin, Y. H.; Liu, G. D. *Electrochem. Commun.* **2010**, *12*, 471−474.
(21) Třesohlavá, E.; et al. *Biomacromolecules* **2010**, *11*, 68−75.
(22) Hui, N.; Sun, X.; Niu, S.; Luo, X. *ACS Appl. Mater. Interfaces* **2017**, *9*, 2914−2923.
(23) Lange, S. C.; van Andel, E.; Smulders, M. M. J.; Zuilhof, H. *Langmuir* **2016**, *32*, 10199−10205.
(24) West, S. L.; Salvage, J. P.; Lobb, E. J.; Armes, S. P.; Billingham, N. C.; Lewis, A. L.; Hanlon, G. W.; Lloyd, A. W. *Biomaterials* **2004**, *25*, 1195−1204.
(25) Liu, N.; Song, J.; Lu, Y.; Davis, J. J.; Gao, F.; Luo, X. *Anal. Chem.* **2019**, *91*, 8334−8340.
(26) Chen, S.; Cao, Z.; Jiang, S. *Biomaterials* **2009**, *30*, 5892−5896.
(27) Ye, H.; Wang, L.; Huang, R.; Su, R.; Liu, B.; Qi, W.; He, Z. *ACS Appl. Mater. Interfaces* **2015**, *7*, 22448−22457.
(28) Liu, N.; Hui, N.; Davis, J. J.; Luo, X. *ACS Sens.* **2018**, *3*, 1210−1216.
(29) Cui, M.; Wang, Y.; Jiao, M.; Jayachandran, S.; Wu, Y.; Fan, X.; Luo, X. *ACS Sens.* **2017**, *2*, 490−494.
(30) Nowinski, A. K.; Sun, F.; White, A. D.; Keefe, A. J.; Jiang, S. *J. Am. Chem. Soc.* **2012**, *134*, 6000−6005.
(31) Geim, A. K.; Novoselov, K. S. *Nat. Mater.* **2007**, *6*, 183−191.
(32) Geim, A. K. *Science* **2009**, *324*, 1530−1534.
(33) Song, Y.; Qu, K.; Zhao, C.; Ren, J.; Qu, X. *Adv. Mater.* **2010**, *22*, 2206−2210.
(34) Wei, H.; Wang, E. *Anal. Chem.* **2008**, *80*, 2250−2254.
(35) Zhou, Q.; Li, G.; Zhang, Y.; Zhu, M.; Wan, Y.; Shen, Y. *Anal. Chem.* **2016**, *88*, 9830−9836.
(36) Dong, Y.; Zhang, H.; Rahman, Z. U.; Su, L.; Chen, X.; Hu, J.; Chen, X. *Nanoscale* **2012**, *4*, 3969−3976.
(37) Li, W.; Wu, P.; Zhang, H.; Cai, C. *Anal. Chem.* **2012**, *84*, 7583−7590.
(38) Li, Y.; Zhu, W.; Kang, Q.; Yang, L.; Zhang, Y.; Wang, Y.; Wei, Q. *ACS Appl. Mater. Interfaces* **2018**, *10*, 38791−38798.
(39) Gagne, R. R.; Koval, C. A.; Lisensky, G. C. *Inorg. Chem.* **1980**, *19*, 2854−2855.
(40) Lin, Y.; Jia, J.; Yang, R.; Chen, D.; Wang, J.; Luo, F.; Guo, L.; Qiu, B.; Lin, Z. *Anal. Chem.* **2019**, *91*, 3717−3724.
(41) Ding, C.; Li, Y.; Wang, L.; Luo, X. *Anal. Chem.* **2019**, *91*, 983−989.
(42) Li, J.; Zhang, S.; Chen, C.; Zhao, G.; Yang, X.; Li, J.; Wang, X. *ACS Appl. Mater. Interfaces* **2012**, *4*, 4991−5000.



DOI: 10.1021/acs.analchem.9b04206
*Anal. Chem.* 2019, 91, 15846−15852